4. Complete Small-Signal Model for Current-Mode Control

4.1 Introduction

In the previous chapter, an accurate continuous-time model was derived for the current-mode control cell with fixed input and output voltages. An invariant gain, $H_e(s)$, was derived for the feedback sampling gain for PWM converters with constant-frequency and variable-frequency control schemes. However, the form of the sampling gain is inconvenient for analytical investigation of the current-mode system since it contains exponential terms in s.

In this chapter, a second-order approximation is made to the sampling gain to provide a model which is accurate to half the switching frequency. The approxi-

mation is in simple polynomial form which will allow the subsequent derivation of analytical transfer functions which are useful for design purposes.

To complete the small-signal model around the current-mode cell, variations in input and output voltages must be allowed. The effects of changes in these quantities will be analyzed in this chapter, and modeled with simple feedforward terms into the duty cycle of the converter. The values of these feedforward terms will be derived for the general PWM switch model, and applied to the three basic two-state converters.

All of the modeling in Chapter 3 has been applied to converters in continuous-conduction mode. The final part of this chapter will cover the modeling of the PWM converters in discontinuous-conduction mode (DCM). It will be shown that no sampled-data modeling is required to derive the model of the DCM converters with current-mode control. All that is needed in the model is the standard DCM switch model, and feedforward terms from the input and output voltages.

4.2 Approximation to Sampling Gain Term

A common expression for all converters was found in Chapter 3 for the sampling gain, $H_e(s)$. This expression is not useful in itself for analytical insight into the

behavior of current-mode systems, and it must be approximated by a simpler function. Fig. 4.1 shows the plot of the exact transfer function, and Fig. 4.2 shows the location of the poles and zeros of the transfer function. The multiple poles of the function are derived from the condition

$$H_e(s_p) = \frac{s_p T_s}{e^{s_p T_s} - 1} = \infty \tag{4.1}$$

The finite solution of this condition is

$$e^{s_p T_s} = 1 \tag{4.2}$$

which is satisfied at frequencies which are integer multiples of the switching frequency. An obvious approach to approximating the transfer function of Eq. (4.1) is to use a continuous-time transfer function with the same poles and zeros in polynomial form. An approximation could then be made at lower frequencies by simply retaining only the lower-frequency poles of the polynomial transfer function. This is not a satisfactory approach. The exponential poles of Eq. (4.1) have infinite Q. However, even at frequencies well before the pole frequency, the phase of the transfer function is significantly altered, as can be seen in Fig. 4.1. Complex polynomial poles with infinite Q exhibit quite different behavior. The phase of a pair of infinite-Q polynomial poles is flat until the resonant frequency, at which point it drops down abruptly by 180 degrees. It does not make sense, therefore, to simply replace the exact expression for $H_e(s)$ with a polynomial expression with coincident poles and zero. Even though both transfer functions

would have the same peaking frequencies, the modeling of the phase characteristic would be very poor.

The objective of a simple model for the sampling gain is to match the gain and phase characteristics of the transfer function as closely as possible over the frequency range of interest. For the sampled-data system, the maximum frequency to be modeled is the Nyquist frequency, equal to half the switching frequency. Notice that the sampling gain function shown in Fig. 4.1 has a well-behaved characteristic up to half the switching frequency, with no discontinuities.

Many different approaches can be taken to match one complex transfer function to another over a prescribed frequency range. However, the sought-after model in the case of current-mode control has some special requirements. At dc, the transfer functions should match exactly, or the resulting new current-mode model would be less accurate at low frequencies than existing averaged models. Secondly, it is known that the oscillation problem inherent in current-mode control occurs at one-half the switching frequency, so the approximation to the transfer function should also be exact here.

A first-pass approximation to the sampling gain is a second-order polynomial. $H_e(s)$ exhibits a change in phase from zero to minus ninety degrees at half the switching frequency, and an increase in gain, as seen in Fig. 4.1. A first-order polynomial is inadequate for modeling such behavior since its maximum possible

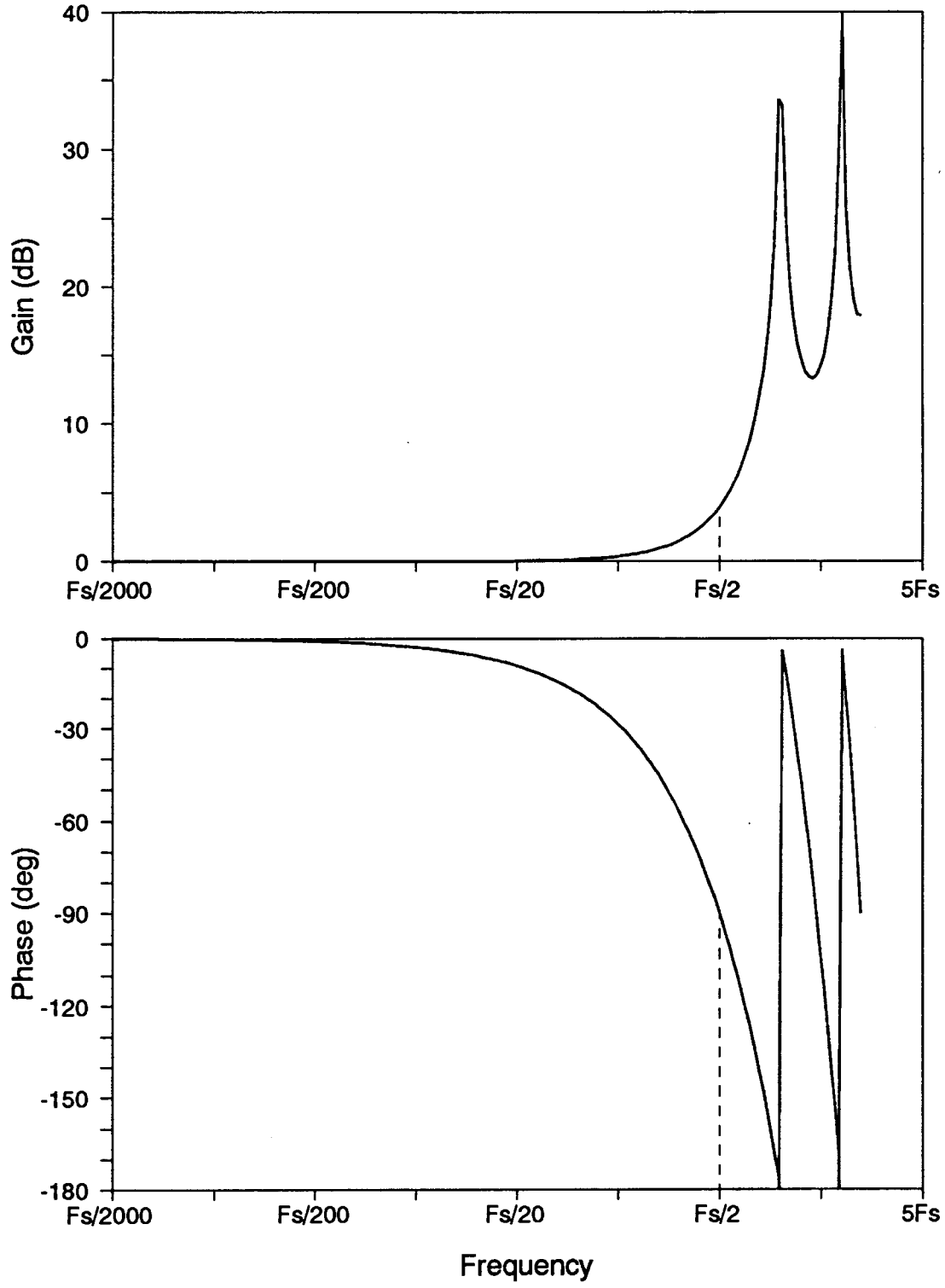

Figure 4.1. ***Exact Transfer Function for Sampling Gain:*** *At half the switching frequency the gain has increased by about 4 dB, and the phase shows exactly 90° lag. High-Q poles are apparent at the switching frequency and twice the switching frequency.*

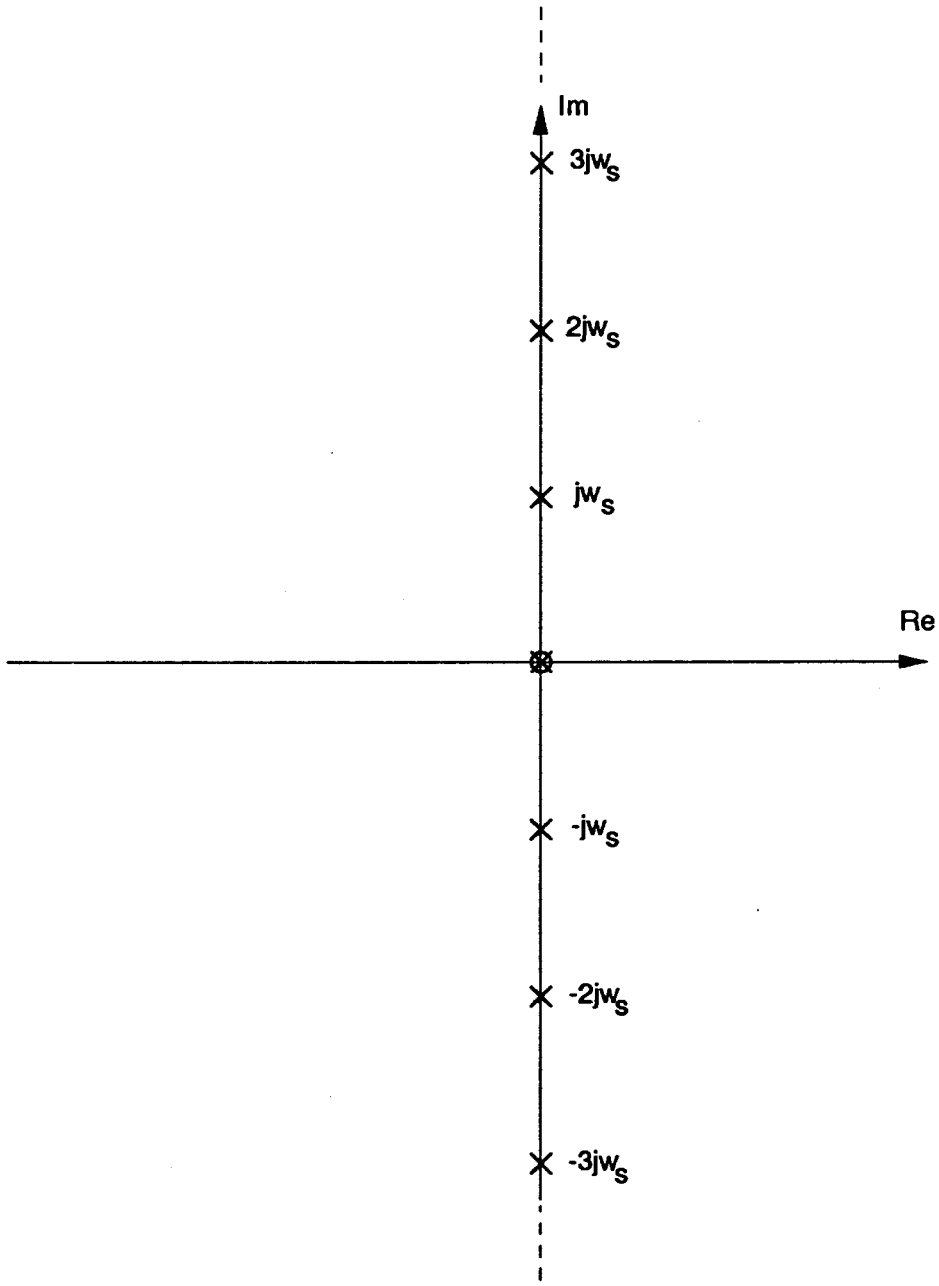

Figure 4.2. ***Pole-Zero Locations of the Exact Sampling Gain:*** *The exact sampling gain transfer function has a pole and a zero at the origin, and an infinite number of complex pole pairs occurring at each integer multiple of the switching frequency.*

phase delay is ninety degrees, obtainable only if the pole or zero is placed at the origin. An approximate expression is chosen such that

$$H_e(s) \simeq 1 + \frac{s}{\omega_n Q_z} + \frac{s^2}{\omega_n^2} \tag{4.3}$$

This approximate expression is equal to unity at dc (s=0), matching the value of the exact transfer function. At half the switching frequency, the approximate expression can be forced to equal the exact transfer function gain and phase exactly if parameters are chosen such that

$$Q_z = \frac{-2}{\pi} \tag{4.4}$$

and

$$\omega_n = \frac{\pi}{T_s} \tag{4.5}$$

This choice of parameters satisfies the end conditions exactly for the approximation, and will suffice if the deviations between the average and exact models are small at all frequencies in between. Fig. 4.3 shows the exact and approximate transfer functions plotted up to half the switching frequency. It can be seen from this figure that the approximate second-order model is very accurate. The gain does not deviate from the exact expression by more than 0.2 dB, and the phase by not more than 3 degrees.

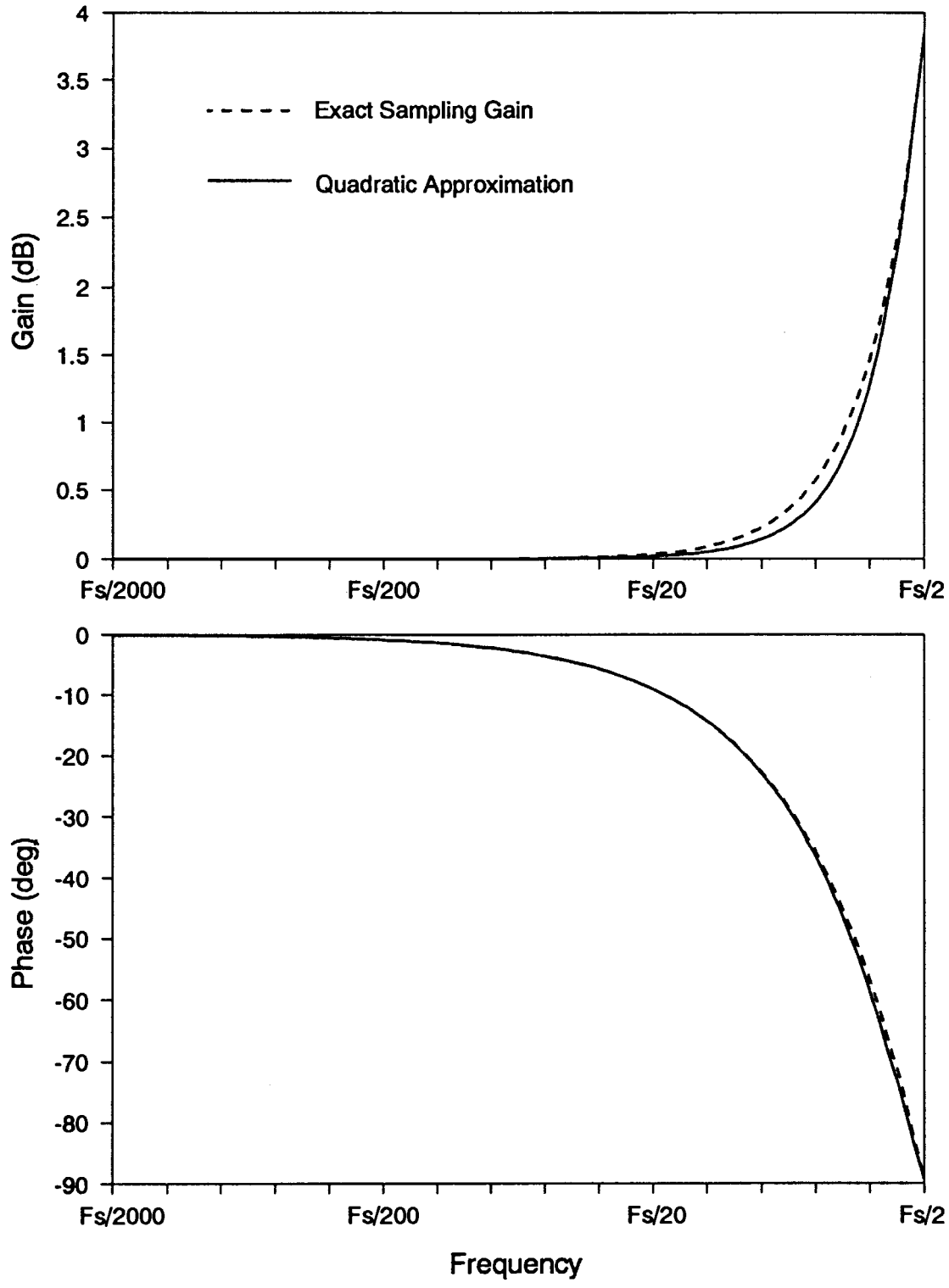

Figure 4.3. ***Exact Sampling Gain and Approximation:*** *The approximate sampling gain expression, given by a quadratic formula, is equal to the exact expression at dc and half the switching frequency, and differs by less than 0.2 dB and 3 degrees at all frequencies in between.*

4.3 Derivation of Feedforward Gains for CCM

The sampled-data model and the low-frequency approximation derived so far have been for the simple current-mode cell with fixed input and output voltages. Perturbations in these voltages must be allowed for to complete the new current-mode model. In current-mode control, it is the peak (or valley) of the current that is directly controlled by the modulator input voltage. It was shown in the previous chapter that perturbations away from steady-state of this controlled current peak lead to perturbations which were held constant over the whole switching cycle. It was not important that the peak current was the controlled quantity.

When deriving the complete current-mode model, however, the fact that the average current is different from the peak current is significant. In Fig. 4.4 the modulator waveforms are shown, and it can be seen that the average current in steady-state is equal to the peak current minus or plus half of the ripple current, depending on the control scheme being used. Furthermore, the ripple current is a function of the duty cycle, input voltage and output voltage of the current cell. As the input and output voltages are changed, there is a direct effect on the duty cycle and the average current value.

The effect of the input and output voltage perturbations can be modeled with the block diagram shown in Fig. 4.5. In addition to the model parameters derived in Chapter 3, feedforward gain terms from the input and output voltages to the duty

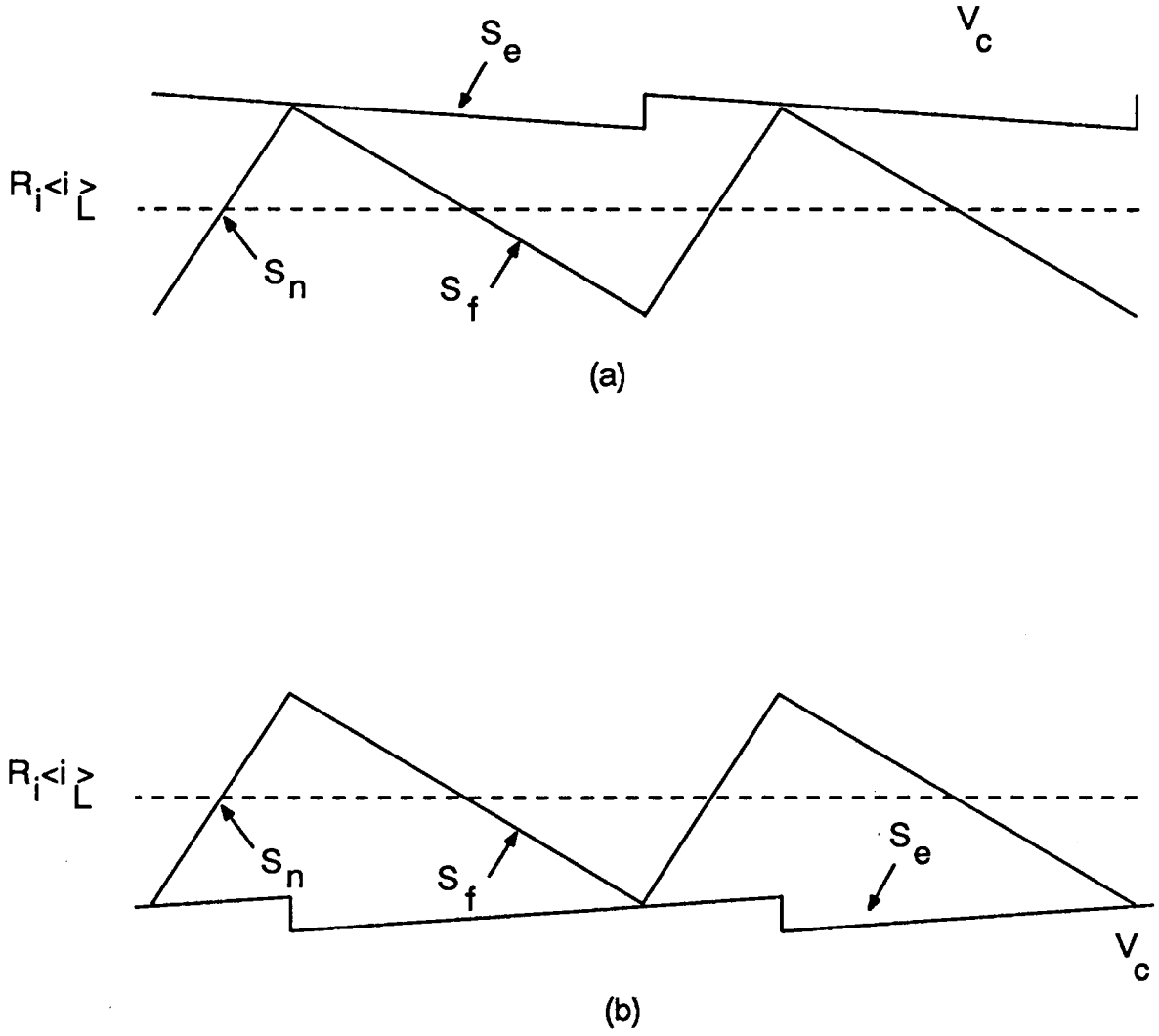

Figure 4.4. Steady-State Modulator Waveforms: *The average inductor current, $\langle i_L \rangle$ is related to the peak current and the ripple current. The ripple current is determined by the voltages across the inductor during the on and off times, and by the duty cycle.*

cycle are included. Notice that the modulator gain is included in the feedforward paths. This is an arbitrary choice which has the benefit of simplifying the expressions for the feedforward terms, and which will provide terms which are independent of the modulator gain parameters. A direct feedforward path from input or output voltage to duty cycle could be chosen, but this produces a more complex gain term which is dependent upon the modulator gain.

The model of Fig. 4.5 is useful for analytical derivation of the system transfer functions, and it is used for this purpose in the next chapter of this dissertation. However, it has the drawback that the gain terms, k_f and k_r, must be derived for each converter to be modeled. An alternative form of the current-mode model is shown in Fig. 4.6. In this representation, the feedforward terms are from the on-time voltage across the inductor, via k_f', and from the off-time voltage across the inductor, via k_r'. This model provides invariant values for these gains which is far more convenient when building the new current-mode model into a circuit analysis program such as Spice.

The models of Figs. 4.5 and 4.6 are, of course, intimately related. The on-time and off-time inductor voltages are linear combinations of the input and output voltages, and the model gains are also linear combinations of each other. By finding the values of k_f' and k_r' of Fig. 4.6, the gains k_f and k_r of Fig. 4.5 can be found with simple algebra. This saves a considerable amount of work in the derivations for each converter. The technique is applied in the analysis of this chapter.

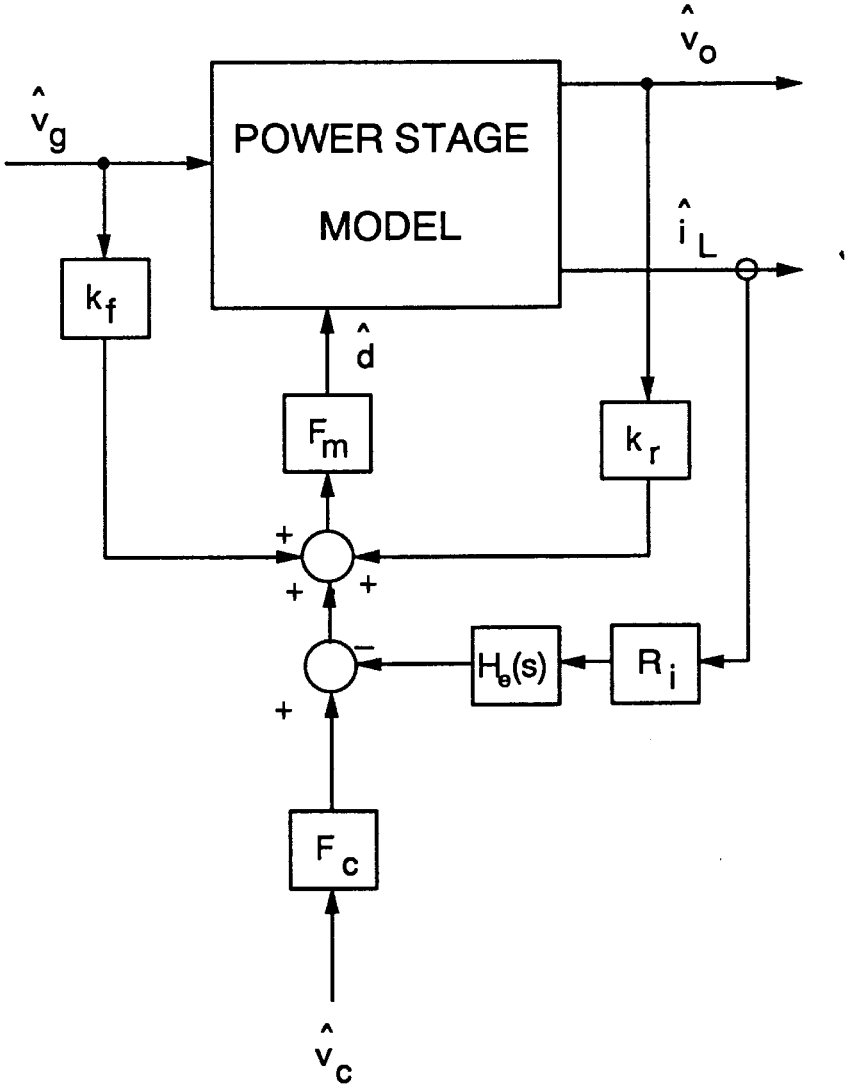

Figure 4.5. ***Complete Small-Signal Model for Current-Mode Control:*** *Feedforward terms from the input and output voltages complete the small-signal model to predict the effect on inductor current of changes in the input and output voltage. This form of the model is useful for transfer-function analysis, and is used in Chapter 5.*

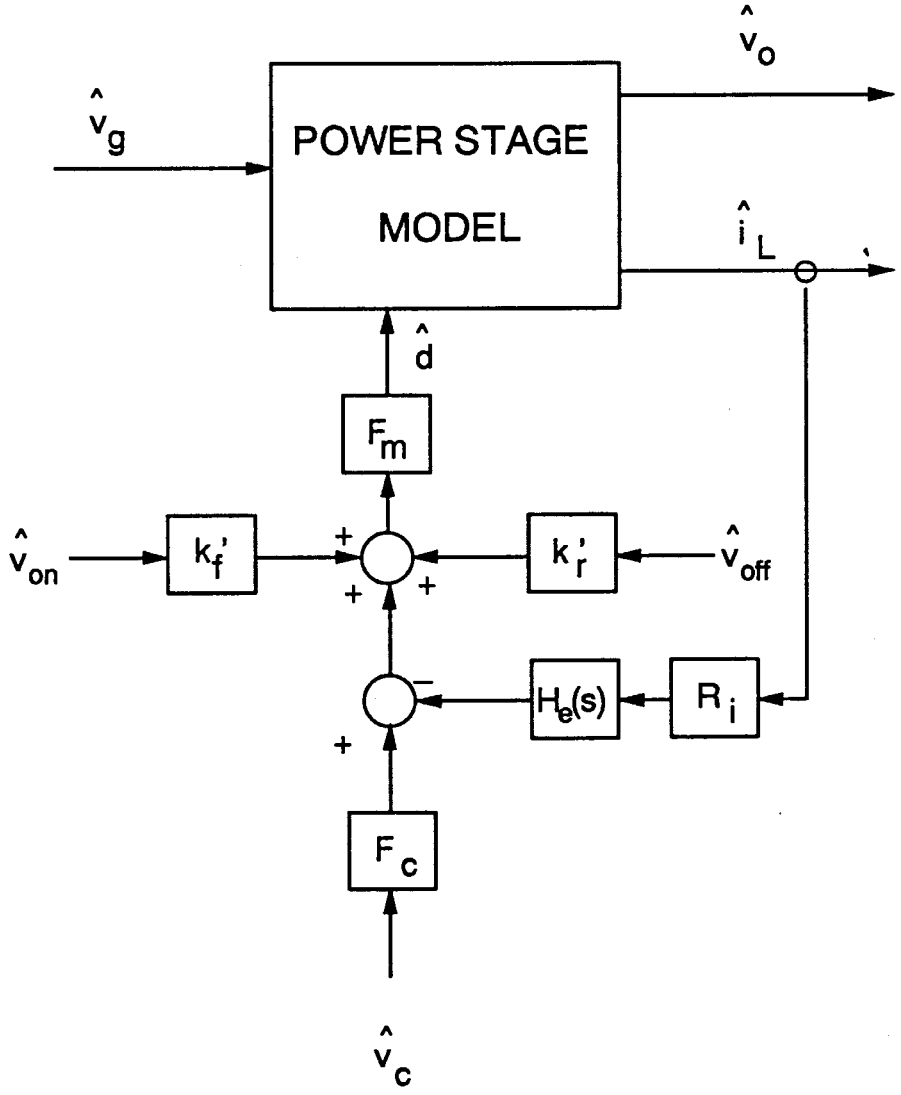

Figure 4.6. ***Invariant Small-Signal Model for Current-Mode Control:*** *Feedforward terms in this model are from the on-time and off-time voltages of the current cell. This form of the model has the advantage of invariance. The values of k_f' and k_r' are constant, regardless of the power stage topology. This is more useful for circuit analysis programs.*

The values of the feedforward terms, k_f' and k_r', can be found from the steady-state equation relating the average inductor current to the peak inductor current. Differentiation of this equation with respect to on-time and off-time voltages (one at a time) gives the small-signal perturbation of average inductor current. The block diagram of Fig. 4.6 can then be analyzed under steady-state conditions, and the value of the feedforward terms chosen to match the correct result.

Referring to the steady-state waveforms of Fig. 4.4, the describing function for the inductor current in terms of the control voltage and operating conditions, for constant frequency control with trailing-edge modulation, or for constant off-time control, is given by

$$R_i < i_L > = v_c - dT_s S_e - \frac{s_f d' T_s}{2} \qquad (4.6a)$$

For constant-frequency, leading-edge modulation and constant on-time control, the describing function is given by

$$R_i < i_L > = v_c + d' T_s S_e + \frac{s_f d' T_s}{2} \qquad (4.6b)$$

The quantity $< i_L >$ denotes the average value of inductor current under steady-state conditions.

The complete small-signal model for the current-mode cell is shown in Fig. 4.7. This model is obtained by inserting the generic current cell of Fig. 3.3 into the

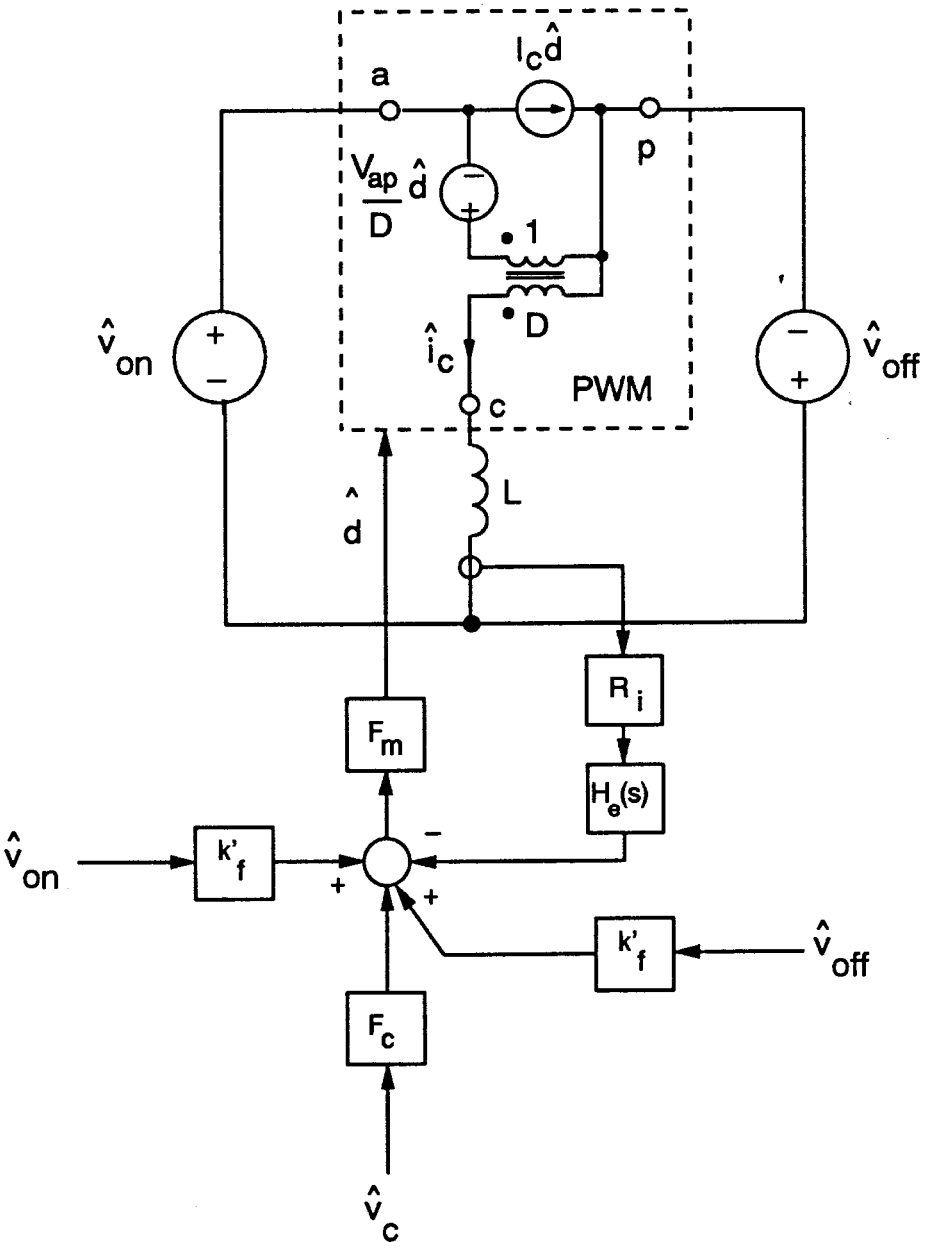

Figure 4.7. ***Small-Signal Model for the Generic Current Cell:*** *The input and output voltages of the generic cell are v_{on} and v_{off}, respectively. For the flyback converter, these are equal to the input and output voltages, and in general are linear combinations of the input and output voltages.*

block diagram of Fig. 4.6. For the generic current-mode cell shown in Fig. 4.7, the following equalities hold:

$$d = \frac{v_{off}}{v_{on} + v_{off}} \tag{4.7}$$

$$d' = \frac{v_{on}}{v_{on} + v_{off}} \tag{4.8}$$

and

$$s_f = \frac{v_{off} R_i}{L} \tag{4.9}$$

Substituting these expressions into the describing function of Eq. (4.6a) for the steady-state average current, and perturbing the on-time voltage, v_{on}, the small-signal perturbation in the average inductor current with respect to the on-time voltage is found for constant-frequency, trailing-edge modulation control:

$$\frac{\hat{<i_L>}}{\hat{v}_{on}} = \frac{DS_eT_s}{V_{ap}R_i} - \frac{D^2T_s}{2L} \tag{4.10}$$

The circuit diagram of Fig. 4.8 can be used to derive the same quantity, this time in terms of the feedforward gain, k_f. The sampling gain term does not appear in Fig. 4.8 since it is unity at dc. The analysis is trivial when one recognizes that the inductor is a short circuit at dc, and the voltage across the inductor is zero

under steady-state conditions. For all forms of current-mode control, the gain is found to be:

$$\frac{\hat{<i_L>}}{\hat{v}_{on}} = \frac{1}{R_i}\left[\frac{D}{F_m V_{ap}} + k_f'\right] \tag{4.11}$$

The two expressions of Eqs. (4.10) and (4.11) can be equated to find the value of the feedforward gain. The value of F_m is dependent upon the form of current-mode control being used, and these values are summarized in Chapter 3. For constant-frequency, trailing-edge control,

$$F_m = \frac{1}{(S_n + S_e)T_s} \tag{4.12}$$

and the feedforward gain is found to be

$$k_f' = \frac{-DT_s R_i}{L}\left[1 - \frac{D}{2}\right] \tag{4.13}$$

A similar procedure is followed for the derivation of the feedforward gain from the off-time voltage. In this case, the describing function for the steady-state average current is perturbed with respect to the off-time voltage, v_{off}, and the small-signal perturbation in the average inductor current with respect to the off-time voltage is found for constant-frequency control to be:

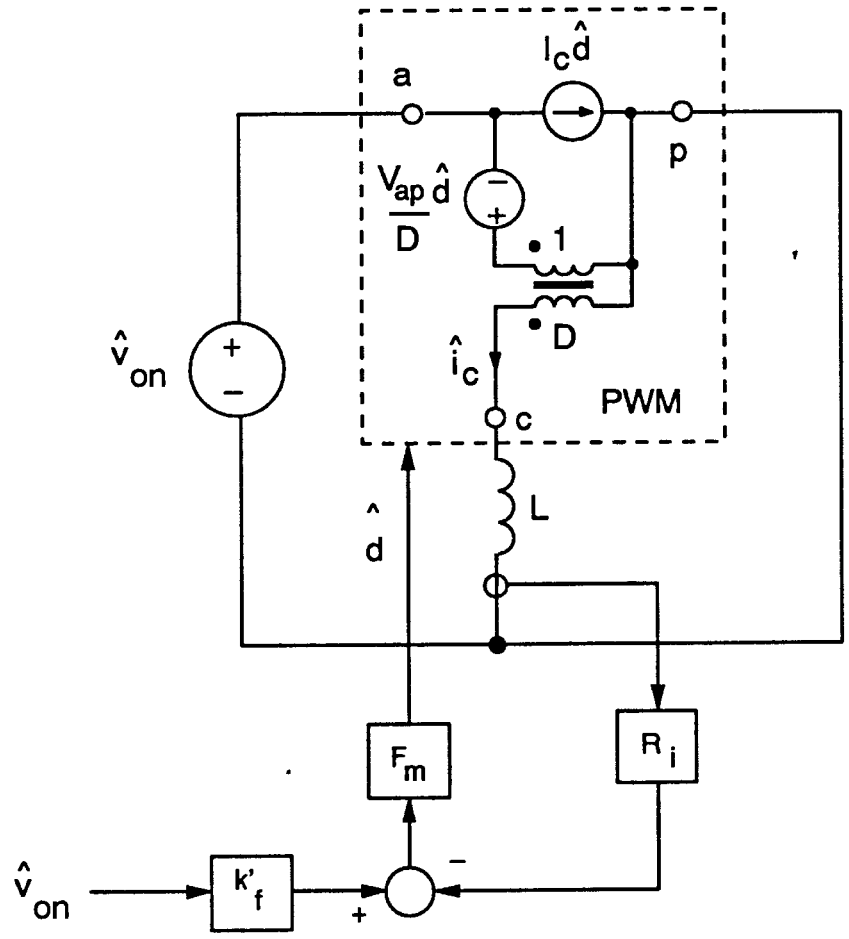

Figure 4.8. ***Generic Current Cell with Fixed Voltage During Off-Time:*** *The on-time voltage, which is in general a linear combination of input and output voltages, is allowed to vary, and the value of feedforward term, k_f', is derived for all converters.*

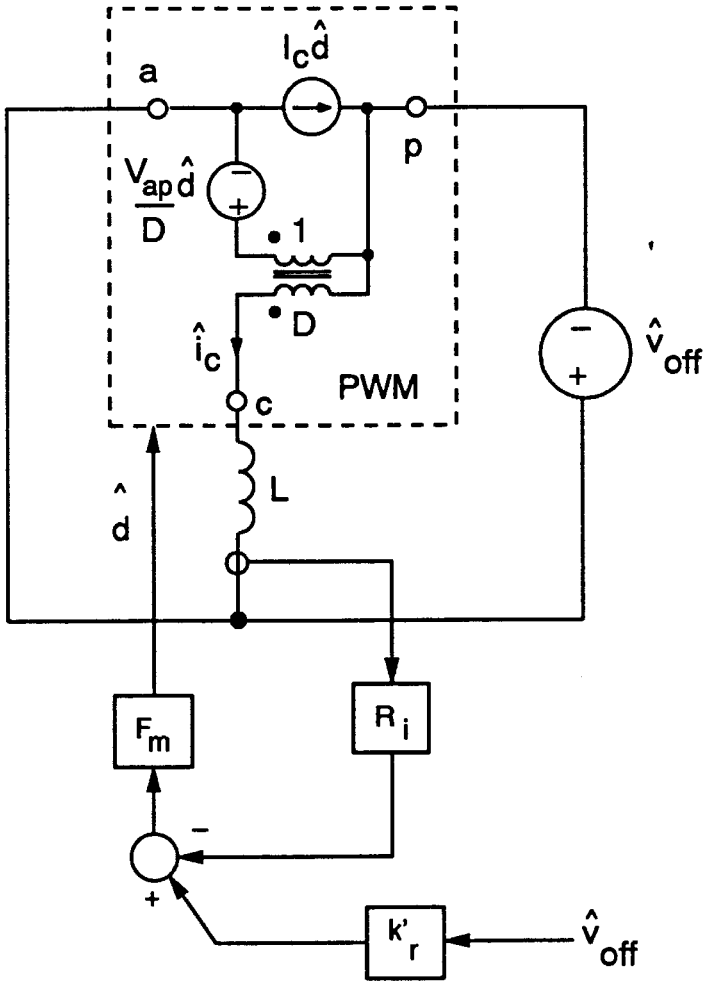

Figure 4.9. ***Generic Current Cell with Fixed Voltage During On-Time:*** *The off-time voltage, again a linear combination of input and output voltages, is allowed to vary in this case, and the value of feedforward term, k_r', is derived for all converters.*

$$\frac{\hat{<i_L>}}{\hat{v}_{off}} = \frac{-D'S_eT_s}{V_{ap}R_i} - \frac{D'^2T_s}{2L} \tag{4.14}$$

The circuit diagram of Fig. 4.9 can also be used to derive the same quantity, this time in terms of the feedforward gain, k_r'. The voltage across the inductor is again zero under steady-state conditions. Using this fact, the gain is found for all forms of current-mode control to be:

$$\frac{\hat{<i_L>}}{\hat{v}_{off}} = \frac{1}{R_i}\left[\frac{-D'}{F_mV_{ap}} - k_r'\right] \tag{4.15}$$

The two expressions (4.14) and (4.15) can be equated to find the value of the feedforward gain from the off-time voltage for constant-frequency control:

$$k_r' = \frac{D'^2T_sR_i}{2L} \tag{4.16}$$

This procedure can be repeated for constant on-time and constant off-time control, and the results for the feedforward gains of the generic current-mode cell are presented in Table 4.1.

Derivation of these gains completes the model of Fig. 4.6, and this model is used in Appendix B of this dissertation to generate equivalent circuit models in PSpice. The gains of the model are also used to derive the feedforward terms of Fig. 4.5 from the input and output voltages. As mentioned before, the on-time and off-

time voltages of the current-mode cell are linear combinations of the input and output voltages. The relationships between these voltages are summarized in Table 4.2 for the three basic PWM converters.

From this table, it can be seen that the on-time voltage for the buck converter is given by $V_g - V_o$, and the off-time voltage is given by V_o. A feedforward path from the input voltage is provided by the feedforward gain k_f' only. Feedforward of the output voltage is provided by both k_f' and k_r'. The specific feedforward gains for the buck converter are therefore calculated from

$$k_f = k_f' = \frac{-DT_sR_i}{L}\left[1 - \frac{D}{2}\right] \tag{4.17}$$

The feedforward gain from the output voltage is found to be:

$$k_r = k_r' - k_f' = \frac{T_sR_i}{2L} \tag{4.18}$$

This process can easily be followed for any PWM converter. The subsequent results for the buck, boost, and flyback converters are summarized in Table 4.3-4.6, where the feedforward gains with different control schemes are given. The derivation of these gains completes the new small-signal model for current-mode control in continuous-conduction mode.

TABLE 4.1
Feedforward Gains for Invariant Current-Mode Model

	Constant Frequency Trailing Edge	Constant Frequency Leading Edge	Constant Off-Time	Constant On-Time
k_f'	$-\frac{DT_s R_i}{L}\left[1-\frac{D}{2}\right]$	$-\frac{D^2 T_s R_i}{2L}$	$-\frac{DT_s R_i}{L}$	$-\frac{DT_s R_i}{2L}$
k_r'	$\frac{D'^2 T_s R_i}{2L}$	$\frac{D'T_s R_i}{L}\left[1-\frac{D'}{2}\right]$	$\frac{D'T_s R_i}{2L}$	$\frac{D'T_s R_i}{L}$

TABLE 4.2
Input and Output Voltage Relationships

	Buck	Boost	Buck-Boost
V_{on}	$V_g - V_o$	V_g	V_g
V_{off}	V_o	$V_o - V_g$	V_o
k_f	k_f'	$k_f' - k_r'$	k_f'
k_r	$-k_f' + k_r'$	k_r'	k_r'

TABLE 4.3
Feedforward Gains for Constant-Frequency, Trailing-Edge Control

	Buck	Boost	Buck-Boost
k_f	$-\frac{DT_s R_i}{L}\left[1-\frac{D}{2}\right]$	$-\frac{T_s R_i}{2L}$	$-\frac{DT_s R_i}{L}\left[1-\frac{D}{2}\right]$
k_r	$\frac{T_s R_i}{2L}$	$\frac{D'^2 T_s R_i}{2L}$	$\frac{D'^2 T_s R_i}{2L}$

TABLE 4.4
Feedforward Gains for Constant-Frequency, Leading-Edge Control

	Buck	Boost	Buck-Boost
k_f	$-\frac{D^2 T_s R_i}{2L}$	$\frac{T_s R_i}{2L}$	$-\frac{D^2 T_s R_i}{2L}$
k_r	$-\frac{T_s R_i}{2L}$	$\frac{D' T_s R_i}{L}\left[1-\frac{D'}{2}\right]$	$\frac{D' T_s R_i}{L}\left[1-\frac{D'}{2}\right]$

TABLE 4.5
Feedforward Gains for Constant Off-Time Control

	Buck	Boost	Buck-Boost
k_f	$-\frac{DT_s R_i}{L}$	$-(1+D)\frac{T_s R_i}{2L}$	$-\frac{DT_s R_i}{L}$
k_r	$(1+D)\frac{T_s R_i}{2L}$	$\frac{D' T_s R_i}{2L}$	$\frac{D' T_s R_i}{2L}$

TABLE 4.6
Feedforward Gains for Constant On-Time Control

	Buck	Boost	Buck-Boost
k_f	$-\frac{DT_s R_i}{2L}$	$-(1+D')\frac{T_s R_i}{2L}$	$-\frac{DT_s R_i}{2L}$
k_r	$(1+D')\frac{T_s R_i}{2L}$	$\frac{D'T_s R_i}{L}$	$\frac{D'T_s R_i}{L}$

4.4 Current-Mode Models for DCM

When operating in the discontinuous mode, the PWM switch model for DCM, shown in Fig. 4.10, must be used. The power stage models are obtained by substituting this model in the circuits of Fig. 4.1. The CCM converters needed sampled-data analysis to develop the small-signal models for current-mode control. This is not the case for converters operating in the DCM region.

Fig. 4.11 shows the modulator waveforms for a converter operating with current-mode control in DCM. The control reference is used with the sensed inductor current to control the turn-off of the power switch. For DCM, the inductor current always starts at zero at turn-on. It is possible to achieve exactly the same effect as current-mode control by using a simple sawtooth ramp whose

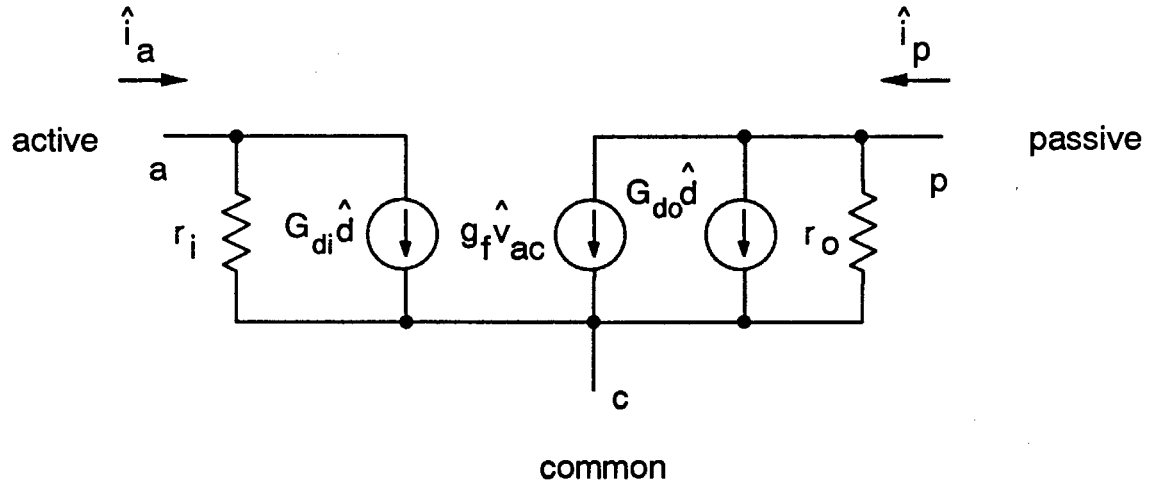

Figure 4.10. ***PWM Switch Model for Discontinuous-Conduction Mode.:*** *The PWM switch model for DCM is different from the model for CCM. It is invariant for all PWM converters.*

slope is determined by the input voltage, output voltage, and inductor value. Inductor current feedback is not necessary. The block diagram of Fig. 4.12 is, therefore, sufficient to completely model the current-mode feedback for DCM. The only task to be done to complete the model is to find the gains, k_f and k_r. As for the CCM model of Fig. 4.5, the model in Fig. 4.12 provides analytical insight, and is used for this purpose in Chapter 5. However, the model of Fig. 4.13 is more practical for circuit modeling since it has invariant gains for all converters. Notice that there is no gain term from the inductor off-time voltage in this model. It is shown below that the gain from this voltage is always zero.

The describing function of the modulator, expressing the on-time in terms of the control voltage and circuit conditions, for converters in DCM with a controlled on-time is given by

$$t_{on} = \frac{v_c}{s_n + S_e} \tag{4.19}$$

The on-time slope, s_n, is a function of on-time voltage, inductor value, and current-sense gain value, R_i. The small-signal perturbation due to changes in on-time voltage can therefore be found by taking the partial derivative of Eq. (4.19) with respect to this voltage. For the current-mode cell, the small-signal gains are given by

$$\frac{\hat{t}_{on}}{\hat{v}_{on}} = \frac{-DR_i}{L} \frac{1}{S_n + S_e} \tag{4.20}$$

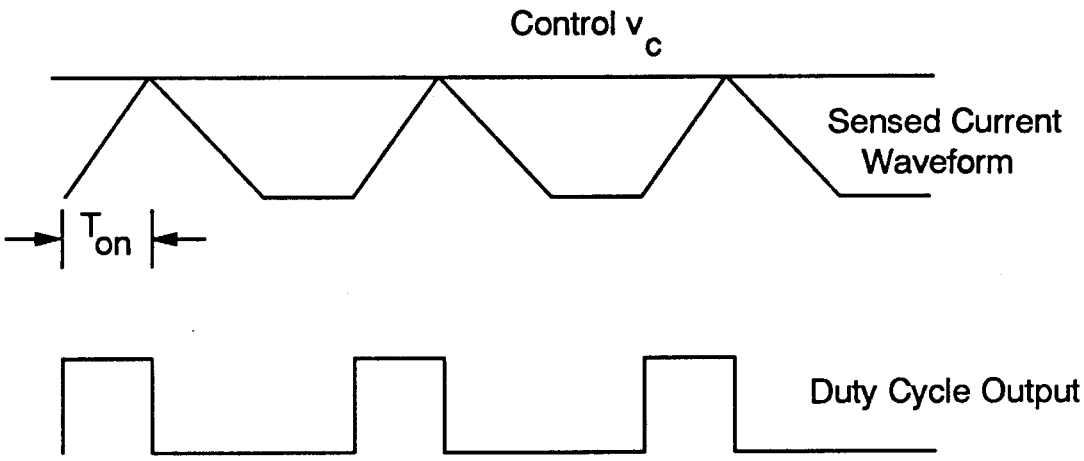

Figure 4.11. ***Discontinuous-Conduction Modulator Waveforms for Current-Mode Control.:*** *The sensed current waveform added to an external ramp is compared with a control signal, v_c, to provide the controlled duty cycle. Notice that the current ramp always starts from zero, and its slope is dependent upon the voltage across the inductor during the on-time.*

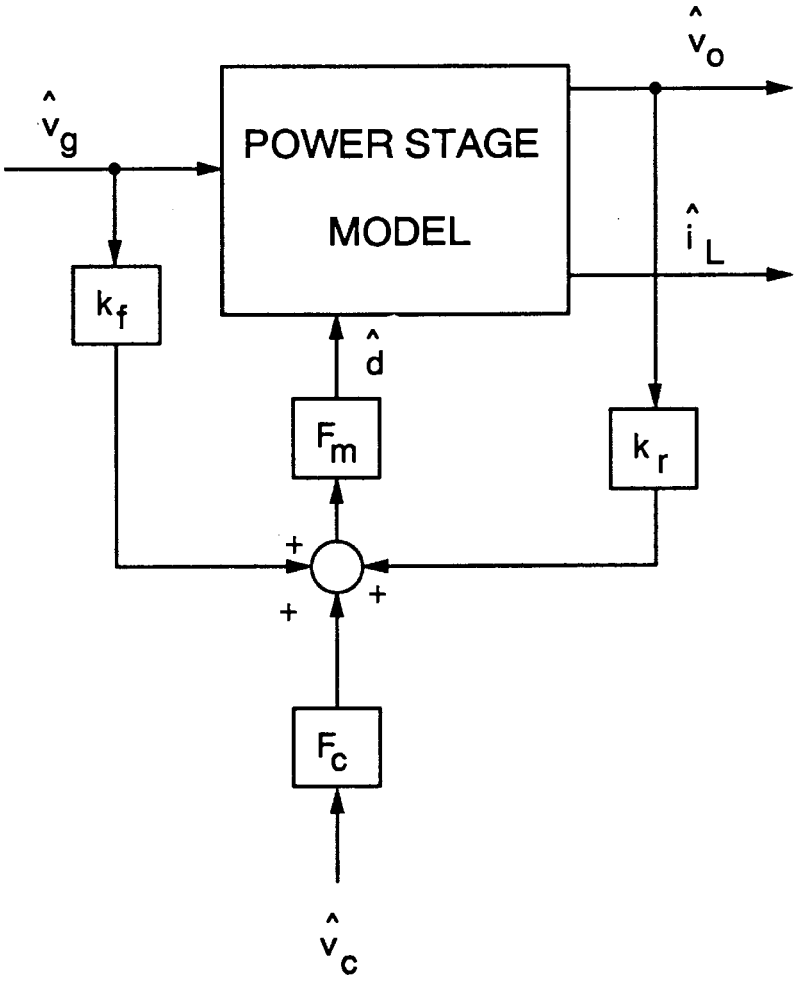

Figure 4.12. Small-Signal Block Diagram for Current-Mode Control (DCM): There is no feedback of inductor current in this block diagram, and no sampled-data modeling is needed. The feedforward blocks, k_f and k_r, provide the necessary control information.

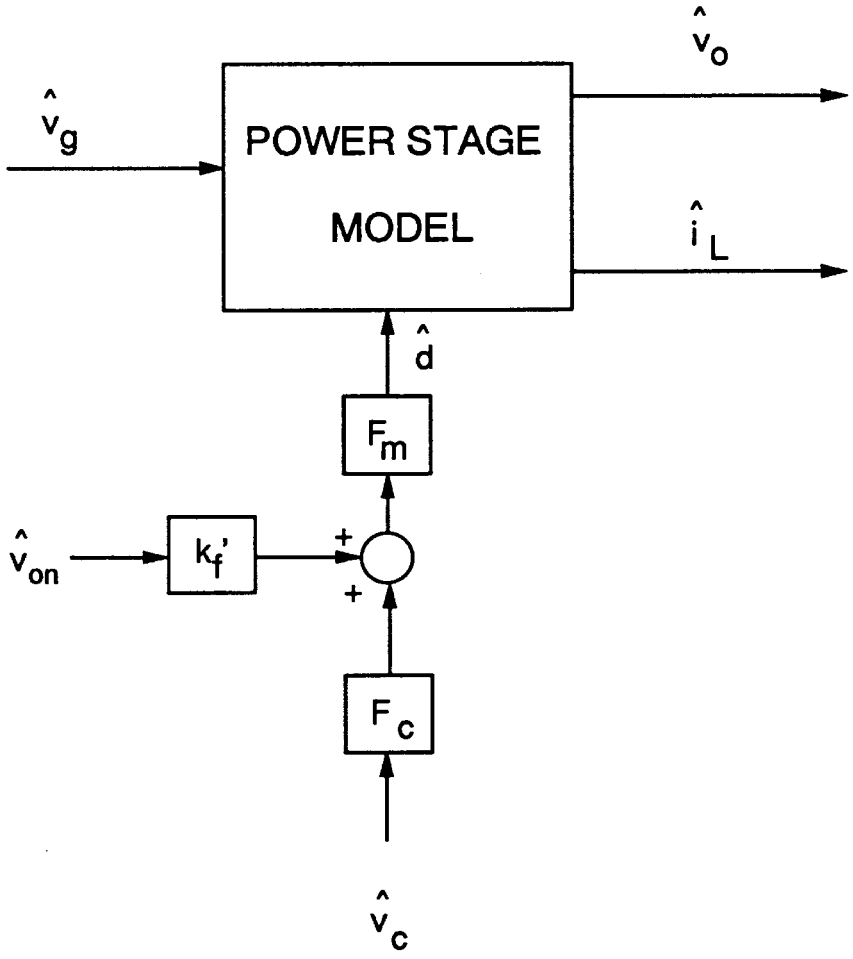

Figure 4.13. Invariant Model for Current-Mode Control (DCM): Only the feedforward gain, k_f', from the on-time voltage is needed in this form of the model. The value of this parameter is the same for all converters being modeled.

and, since the on-time does not depend upon the off-time slope,

$$\frac{\hat{t}_{on}}{\hat{v}_{off}} = 0 \tag{4.21}$$

For constant-frequency control, the perturbations in duty cycle are then given by

$$\frac{\hat{d}}{\hat{v}_{on}} = \frac{-DR_i}{L} \frac{1}{(S_n + S_e)T_s} \tag{4.22}$$

and

$$\frac{\hat{d}}{\hat{v}_{off}} = 0 \tag{4.23}$$

For constant off-time control, the gains with respect to the duty cycle are

$$\frac{\hat{d}}{\hat{v}_{on}} = -\frac{D'DR_i}{L} \frac{1}{S_n T_s} \tag{4.24}$$

and

$$\frac{\hat{d}}{\hat{v}_{off}} = 0 \tag{4.25}$$

Constant on-time current-mode control, and constant-frequency with leading-edge modulation cannot be implemented since there is no current signal available at the end of the off-time in DCM.

In the model of Fig. 4.13, perturbations in the duty cycle are given by the product of the gain k_f' and the modulator gain, F_m. This representation provides a more

convenient model. The necessary gains can be found by dividing Eqs. (4.22) and (4.24) by the modulator gain, resulting in the same expressions for both constant frequency and constant off-time control.

$$k_f' = -\frac{DT_sR_i}{L} \tag{4.26}$$

The gains for the generic current-mode cell can be translated into specific gains for each of the converters by using the relationships between the input and output voltages summarized in Table 4.2. The results of the analysis are presented in Table 4.7, for both constant-frequency and constant off-time control. Modulator gains for these control schemes, repeated here for convenience, are the same as those for continuous conduction mode.

TABLE 4.7

Summary of Gain Parameters for DCM

	Buck	Boost	Buck-Boost
k_f	$-\frac{DT_s R_i}{L}$	$-\frac{DT_s R_i}{L}$	$-\frac{DT_s R_i}{L}$
k_r	$\frac{DT_s R_i}{L}$	0	0
F_m	$\frac{1}{(S_n + S_e)T_s}$ (Constant Frequency) $\frac{D'}{S_n T_s}$ (Constant Off Time)		
F_c		1 (Constant Frequency) $e^{sDT_s/2}$ (Constant Off Time)	

4.5 Conclusions

The complex expression for the sampling gain, $H_e(s)$, derived in Chapter 3 was simplified with an approximate expression. A second-order polynomial was sufficient to accurately model the effects of the sampling action of current-mode control up to half the switching frequency. The approximate sampling gain is given by

$$H_e(s) \simeq 1 + \frac{s}{\omega_n Q_z} + \frac{s^2}{\omega_n^2} \tag{4.27}$$

where

$$Q_z = \frac{-2}{\pi} \tag{4.28}$$

and

$$\omega_n = \frac{\pi}{T_s} \tag{4.29}$$

This simple transfer function gives remarkable accuracy in approximating the exact transfer function, both in gain and phase predictions. At dc and half the switching frequency, the functions are identical. It is not surprising that the second order transfer function is adequate, since the nature of the problem in the current-feedback system is an oscillation, normally associated with a pair of complex poles in the system. It will be seen in the next chapter how the complex zeros of the approximation to the sampling gain produce a corresponding pair of complex poles in the closed-loop system. An interesting feature of the sampling gain approximation is that it has complex zeros in the right-half plane. The im-

portance of this in modeling system performance will also be discussed in the next chapter.

The small-signal model for continuous-conduction mode was completed with the derivation of feedforward gains from the on-time and off-time voltages across the inductor. These gains were then used to derive the individual feedforward gains for specific converters from the input and output voltages. The invariant form of the model with feedforward from on-time and off-time voltages is very useful for circuit modeling. The model with feedforward from input and output voltages can provide more analytical insight into some of the observed phenomena of current-mode control. The impact of the feedforward gains on the small-signal performance will be discussed in the next chapter.

Finally, the small-signal model for current-mode control with discontinuous inductor current was derived. Simple arguments show that a current-feedback loop is not even needed in the small-signal model, and sampled-data analysis is not needed for the DCM model. Feedforward gain terms provide the complete model for the system when coupled with an accurate model for the power stage.

Power supply trouble?

4-Day Lab Design Workshops in the US and Europe

Need help with your current project? Want to become a more efficient designer? Our mission is to teach and clarify the power supply design process. Regardless of the power converter you are working on, this essential hands-on course will provide the needed skills in topologies, magnetics, and control to be a much more focused and efficient designer. Design and build two real-world converters at 25 W and 60 W in the afternoon laboratory, and measure ringing waveforms and efficiency. Intensive voltage-mode and current-mode models and design procedures are given and confirmed in the lab.

New: digital control introduction
As part of the control series, Dr. Ridley will give an introduction to digital control. He will discuss where apply it, the advantages and disadvantages, and the impact on your project.

Visit our website to register. WWW.RIDLEYENGINEERING.COM

RIDLEY ENGINEERING

Ridley Engineering, Inc. 3547 53rd Ave W, Suite 347 Bradenton, FL 34210 +1 941-538-6325
Ridley Engineering Europe SAS Rue St Joseph 24540 Monpazier, France +33 553278720